Proceedings of
ASME TURBO EXPO 2001
June 4-7, 2001, New Orleans, USA

2001-GT-143

STUDIES ON COOLING AIR EJECTED OVER A CORRUGATED WALL : ITS AERODYNAMIC BEHAVIOR AND FILM EFFECTIVENESS

K. Funazaki
Iwate University
Morioka, Japan

T. Igarashi, Y. Koide and K. Shinbo
Ishikawajima-Harima Heavy Industries Co.
Tokyo, Japan

ABSTRACT

This paper describes experimental studies on aerodynamic behaviors of the air ejected from several discrete hole rows on a corrugated wall and the resultant film effectiveness over the wall. The corrugated wall is a model of an air-cooled liner surface for aero-engine augmentors. Measurements on the aerodynamic aspects are conducted by use of a pneumatic five-hole probe in order to clarify the features of the ejected air over the corrugated wall. The temperature field is examined by traversing a thermocouple, which also reveals the behavior of the ejected air. Film effectiveness associated with the air-ejection is then determined from the extrapolation of the measured temperature profile. It is accordingly found that the air jets near the ejection holes behave like those from the holes on a flat-plate, being accompanied by upward and downward secondary flows around the jets. Close inspections on the behavior of the jets also reveal that the jet cores tend to diminish much faster than those in the flat-plate case, which is probably due to a mixing of the high-momentum jet and low-momentum air on the 'valley' of the corrugated wall. Such characteristics of the jets result in transversely uniform distribution of the temperature which is favorable to the liner surface protection from the extremely hot gas.

INTRODUCTION

Because of its chaotic turbulent flow feature as well as its potential for heat transfer enhancement, a number of efforts have been devoted to studies on thermo-fluid characteristics of the flow over a corrugated plate and/or inside a corrugated pipe (Henn and Sykes [1], Lee et al. [2], Russ and Beer [3], Sugiyama et al. [4], Ohta et al. [5]). However, little attention is paid to the inside of an augmentor of supersonic aircraft engines, where reheated exhaust gas from the turbine is flowing over the corrugated liner surface of the augmentor (see Figure 1). The corrugated liner, which has high specific rigidity and can endure large buckling loads, operates under extremely severe thermal conditions and needs to be effectively air-cooled with less coolant consumption. Film cooling or effusion cooling is usually applied to the liner, however, almost all the previous studies concerning with the film cooling dealt with that on a flat plate, concave or convex wall and very few have been reported on the film cooling over a corrugated wall except for studies done by Shinbo et al. [6]. Therefore less information is available for optimizing the film cooling configuration of a corrugated liner to reduce the cooling air consumption.

This paper therefore reports on experimental studies that investigated aero-thermo characteristics of secondary air ejected into the primary flow from several discrete cooling holes on a test model with corrugated surface. The model geometry was taken from an augmentor liner of an aeroengine that was under development. A pneumatic five-hole probe measured the three-dimensional flow structure associated with the ejected air. After the secondary air was heated, a thermal probe then examined the temperature field over the corrugated surface. Using an extrapolation of the measured temperature data, film effectiveness on the wall was estimated.

Nomenclature

A	: amplitude of the wave in corrugated wall
d	: diameter of a cooling hole
m	: blowing ratio (= $\rho_2 U_2 / \rho_\infty U_\infty$)
p	: spanwise pitch of the cooling hole
Re	: Reynolds number (= $U_\infty \lambda / \nu$)
T	: temperature
T_2, T_∞	: secondary flow temperature, main flow temperature

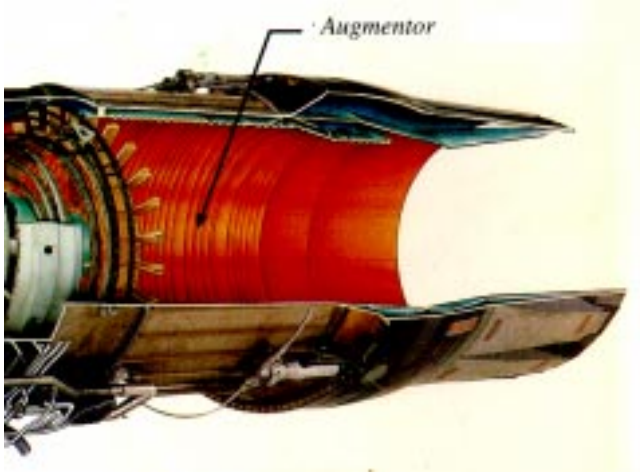

Figure 1 Corrugated augmentor liner(F100-PW-220)

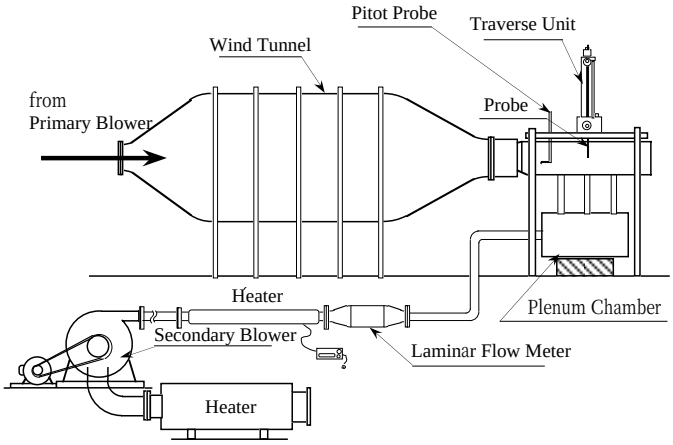

Figure 2 Test apparatus

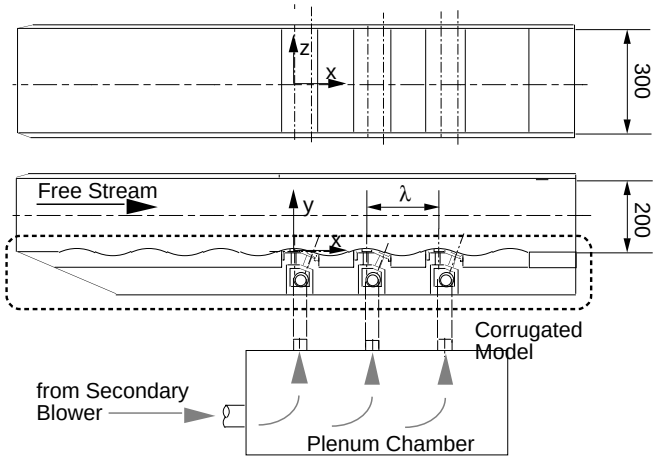

Figure 3 Test model with aecondary air ejection system (unit : mm)

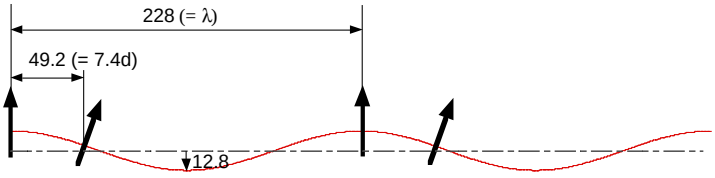

Figure 4 Dimensions of corrugated surface and the locations of cooling air ejection hole (unit : mm)

T_{ad} : adiabatic wall temperature
U_2, U_∞ : jet velocity from the cooling hole, main flow velocity
u, v, w : velocity components
x, y, z : coordinates in longitudinal, upward and transverse directions
λ : wavelength of the corrugated wall
ν : kinetic viscosity
η, η_{wall} : non-dimensional temperature, film effectiveness
ρ_2, ρ_∞ : density of the secondary flow, density of main flow

EXPERIMENTS

Test Apparatus

Figure 2 shows the test apparatus. Main flow from the primary blower passed through the settling chamber and contraction nozzle before entering the test model whose detail is depicted in Figure 3.

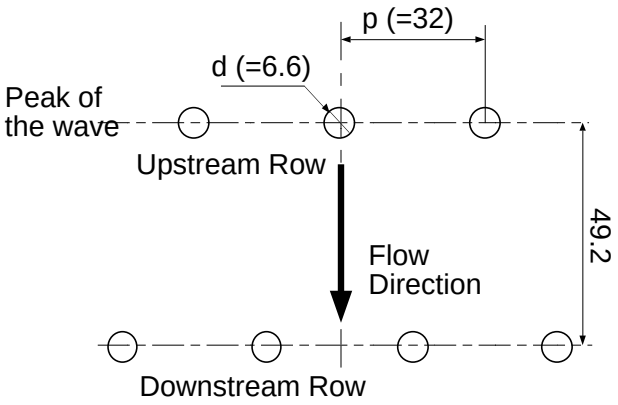

Figure 5 Cooling hole configuration (unit : mm)

The test model was manufactured from Plexiglas. The cross section of the test model was 300 mm width and 200 mm average height, and the leading edge of the test model was sharp-edged. Since the cross section of the nozzle exit was slightly larger than that of the test model, small amount of air was discharged, which helped the boundary layer restart from the inlet of the test model. Secondary air came from the secondary blower via a laminar flowmeter and two heaters to the plenum chamber that was attached to the bottom of the test section. These two heaters were used only in the temperature measurement to increase the secondary air temperature by about 20 K.

The test section was provided with a corrugated bottom wall that consisted of three upstream waves with no cooling holes on the first half of the test section and three downstream waves with two rows of cooling holes on each of the waves. Dimensions of the corrugated wall are shown in Figure 4, along with the locations of the air ejection holes. The shape of the waves was almost sinusoidal with wavelength λ and amplitude A of 228 mm and 12.8 mm, respectively. The cooling hole configuration is displayed in Figure 5. The cooling hole diameter d was 6.6 mm and hole pitch in each row was 32 mm (4.8d). The upstream row of the cooling holes was on the peak of the surface wave and the other row located 49.2 mm (7.4 d) downstream. The center hole of the upstream row located at the transverse center of the test model, while the cooling holes of the downstream row were staggered by a half pitch. Air ejection angles with respect to the main flow direction were 90 deg for the upstream row and about 70 deg for the downstream row. The secondary air was carefully delivered almost equally to each of the three waves from the plenum chamber through flexible connection pipes. However, due to the nonuniform pressure distribution along the streamwise direction, it was not possible to equalize coolant mass fluxes from upstream and downstream rows of the cooling holes.

As for the coordinate system, x-, y- and z-coordinates were in the longitudinal (streamwise), upward and transverse directions of the test model, respectively.

Instruments

Aerodymanic measurements were conducted using a 5-hole probe that was connected to pressure transducers with high precision (Kyowa PDL-40GB). This probe had a small sensing head with large opening above the head for minimizing blockage effect of the probe. Careful calibration using a small calibration tunnel determined the probe angular characteristics which correlated pitch and yaw angles of the flow and the sensed pressure data using two-variable polynomial expressions. Similar expressions were derived for obtaining stagnation pressure as well as velocity magnitude of the flow from the pressure data. Measurable zone by this probe was about ± 30 deg in pitch and yaw angles. Inlet stagnation pressure was obtained from a Pitot probe placed

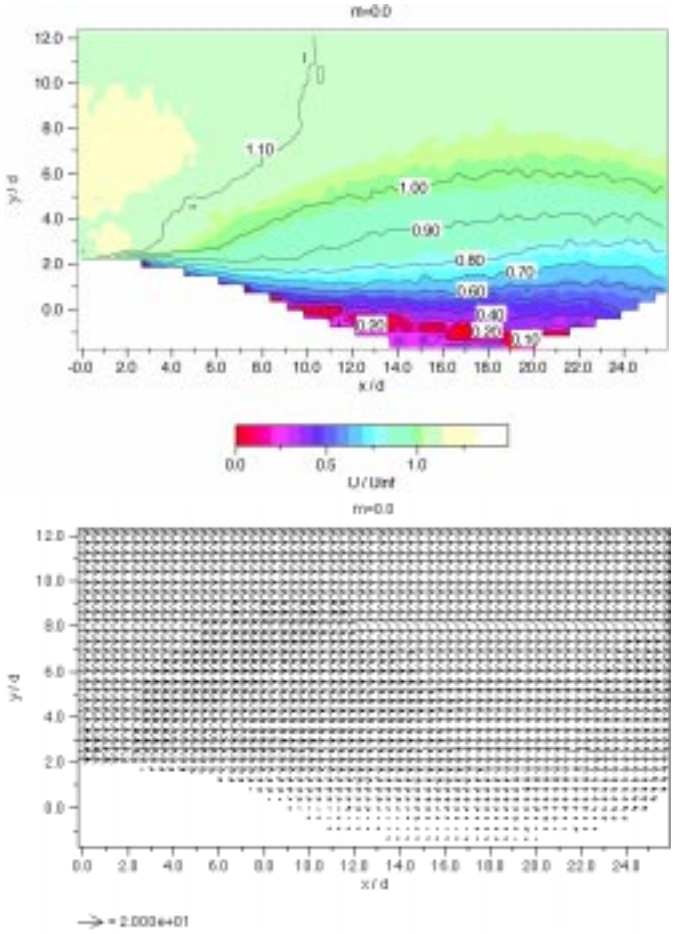

Figure 6 Velocity measurement on x-y plane for m=0 (upper) magnitude contour (lower) velocity vectors

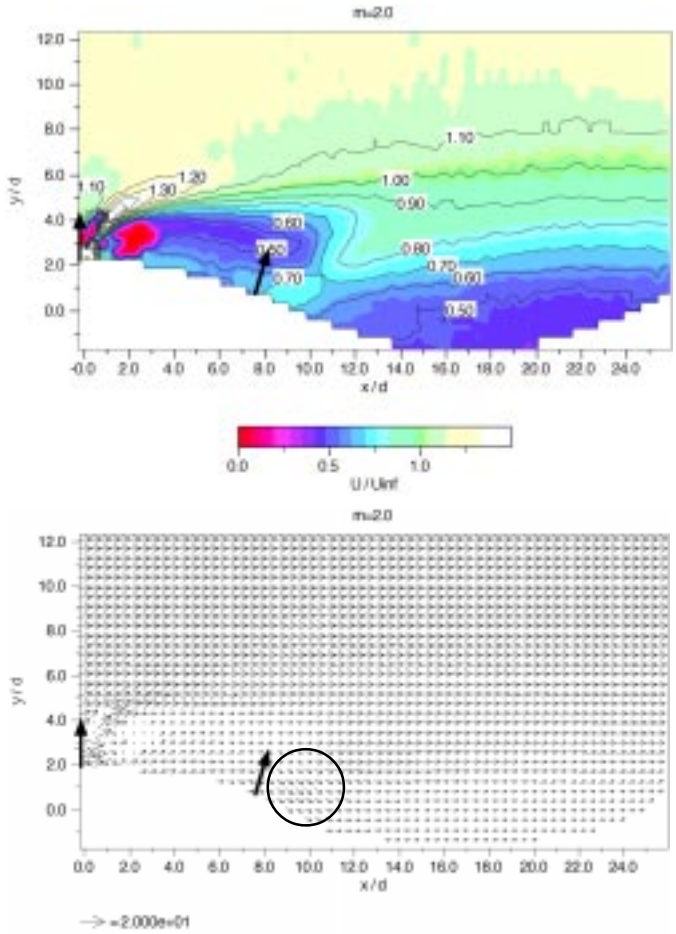

Figure 7 Velocity measurement on x-y plane for m=2.0 (upper) magnitude contour (lower) velocity vectors

at the inlet of the test model. A PC-controlled traversing mechanism was employed to settle the probe to a specified position. This PC also controlled a data acquisition system for the pressure measurement as well as the temperature measurement described in the following.

After reaching a thermal equilibrium condition of the heated air in the plenum chamber, temperature measurements over the corrugated wall were executed using a thermal probe that was installed in the above-mentioned traversing mechanism. The plenum chamber was equipped with a thermocouple to obtain a reference temperature for determining film effectiveness, while main flow temperature was measured at the inlet of the test model.

A single hot-wire probe was also employed at the inlet of the test section to determine the level of inlet free-stream turbulence intensity.

Measurement Region

Aerodynamic and temperature measurements were conducted on seven transverse or y-z planes for one wavelength of the corrugated wall as shown later in Figure 8, and one longitudinal or x-y plane containing the centerline of the test model. The streamwise distance of the y-z planes measured from the peak of the wave (x/d) was 0.0 (A), 3.03(B), 6.05(C), 9.08(D),12.10(E), 18.15(F) and 24.21(G). Each of the measurement planes extended from z/d = -6.1 to z/d = 6.1 in the spanwise direction and from (wall surface + 0.76 d) to y/d = 12.1 in the crossflow direction. The area covered in the temperature measurement was smaller than that used in the aerodynamic measurement, which extended from z/d = -4.5 to z/d = 4.5.

Test Conditions

The flow field concerned was characterized by Reynolds number of the main flow (Re) and blowing ratio or mass flux ratio of the ejected air (m). Reynolds number in this study was based on the inlet velocity U_∞ and the wave length of the corrugated wall λ , which was defined as

$$Re = U_\infty \lambda / \nu \qquad (1)\ .$$

The blowing ratio was given by

$$m = \rho_2 U_2 / \rho_\infty U_\infty \qquad (2)\ ,$$

where ρ_2 was the density of the secondary air based on the condition inside the plenum chamber, U_2 was the average jet velocity that was calculated from the mass flow rate of the secondary flow divided by total area of the cooling holes. In the present study the Reynolds number was about 1.6×10^5 and the blowing ratios adopted were 2.0, which was close to the design value, and 4.0. Free-stream turbulence measured at the inlet of the test section was 1%.

Data Reduction

As mentioned above, time-averaged three dimensional flow structure was obtained by the 5-hole probe, which yielded velocity vectors on the measurement planes. From the measured temperature, non-dimensional temperature η was calculated as

$$\eta = \frac{T - T_\infty}{T_2 - T_\infty} \qquad (3)\ .$$

Film effectiveness is an important information for the cooling design of the corrugated liner. However, the test model used in this study was not equipped with any thermocouples on its surface, thus the only way to evaluate the film effectiveness associated with the air ejection was to take advantage of the temperature data measured above the test model. Since the test model was made from Plexiglas of large thickness and low thermal conductivity, the wall surface could be regarded as adiabatic wall except for the near-jet region. In fact, gradual temperature distributions were observed near the corrugated wall in the temperature measurements, which will be described later. This enabled the authors to estimate adiabatic wall temperature T_{ad} from the extrapolation of the measured temperature, assuming a parabolic distribution as the temperature profile at the near-wall region. Then film effectiveness on the corrugated surface η_{wall} could be calculated by

$$\eta_{wall} = \frac{T_{ad} - T_\infty}{T_2 - T_\infty} \qquad (4).$$

It has turned out that the present study yielded similar film effectiveness distributions as those obtained in the previous study (Shinbo et al. [6]), where the test model with a number of thermocouples flush-mounted on the surface was employed to determine the film effectiveness.

Uncertainty Analysis

Uncertainty associated with flow measurements using 5-hole probe originated mostly from uncertainties in the reference flow velocity at the calibration as well as in the resultant correlations expressed by 4-th order two-variable polynomials. Using the method of Kline and McClintock [7], it was estimated that errors in the magnitude and pitch/yaw angle of the measured velocity vectors were about $\pm 3.5\%$ and $\pm 2.0\%$, respectively.

It was also found that error in the measured temperature by the thermocouple was about $\pm 0.3°C$. This led to about $\pm 5\%$ error in η near the ejected jets, while the error increased up to about $\pm 10\%$ with increased distance from the jets. Meanwhile, a rough estimation revealed that error in the adiabatic wall temperature T_{ad} was about $\pm 0.7°C$, which resulted in about $\pm 8\%$ error in the film effectiveness η_{wall} at the near-jet region and about $\pm 14\%$ error at the further downstream of the jets.

RESULTS

Aerodynamics of the Ejected Air

Measurements on x-y plane Figure 6 shows contours of the velocity magnitude normalized by the inlet velocity magnitude (U_∞) and velocity vectors obtained on the x-z measurement plane for m = 0.0. The appearance of a region with very low speed over the valley of the corrugated wall indicated that the flow separation occurred over the region apparently from x/d = 10 to x/d = 22, although the probe used in this study could not detect any reversed flow. The velocity vectors in the lower part of Figure 6 also supported this judgment. The flow field drastically changed when the secondary air ejected from the cooling holes, as shown in Figure 7 (m = 2.0). In this case the air emerged from all the cooling holes. Since the measurement plane was aligned with the centerline of one of the upstream holes, high speed region associated with the jet was clearly seen on this contours. One might notice that a widespread wake region appeared behind the upstream jet, which extended in the streamwise direction from just downstream of the jet to x/d = 10. The other feature of the flow field with the air ejection was that the separation zone over the valley, which was characterized with very low speed in Figure 6, almost disappeared. This was also identified in the plot of the velocity vectors. There emerged prominent downwash behind the downstream hole as marked with a circle, which contributed to the disappearance of the separated zone, as discussed later in this paper.

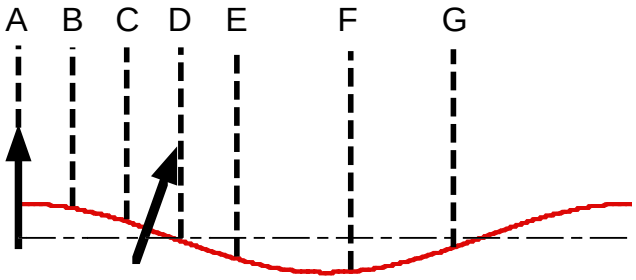

Plane	Axial Location (x/d)	Wall Intersection (y/d)
A	0.00	1.94
B	3.03	1.71
C	6.05	1.01
D	9.08	-0.21
E	12.10	-1.27
F	18.15	-1.92
G	24.21	-0.70

Figure 8 Locations of y-z measurement planes

Measurements on y-z planes Figure 8 displays the streamwise locations of y-z measurement planes named with A to G from the upstream. Each of the planes intersected the corrugated surface at y/d = 1.94 (plane A), = 1.71 (plane B), = 1.01 (plane C), =-0.21 (plane D), =-1.27 (plane E), =-1.92 (plane F) and = -0.70 (plane G), respectively. First, for the sake of better understanding of the jet behavior over the corrugated wall, measurements on those planes were executed on the air ejected from a single cooling hole row (upstream or downstream row), which was followed by the investigations of the air ejection from all the cooling holes.

Single Row Ejection Figure 9 shows the results obtained on each of the measurement planes for the upstream row ejection case with m = 2.0, which are the contours of the velocity magnitude and the secondary velocity vectors associated with the air ejection from the cooling holes. Behind the jets from the upstream cooling holes, wake regions with very low speed clearly appeared on plane B, while high speed regions occurred around the wakes. As seen in the previous studies on jet behavior in a crossflow, such as Leylek and Zerkle (8), two counter rotating vortices arose inside each of the jets, yielding downwash between the two neighboring jets and upward velocity beneath the wakes. Due to this vortical motion, the wake behind the jet became rounded. As already confirmed in Figure 7, the ejected air was indistinguishable by the location of plane C, and the vortical structure associated with the jet attenuated as well. It is worth mentioning that the downwash observed outside the jet wakes relatively weakened in comparison with the upward motion inside the wakes. This tendency became more enhanced on plane D, despite that the wall surface was descending there. The low speed regions took a *grave stone* shape whose root section tended to expand approaching to its neighboring wakes. The velocity field became nearly uniform up to the streamwise location of plane F.

Figure 10 depicts the velocity fields measured on plane E and plane F for the case where the secondary air was ejected only from the downstream row of the cooling holes. For help in understanding the air ejection effect, the velocity field measured on plane E for no air ejection condition was also shown in Figure 11. Note that there appeared slight spanwise fluctuation in the velocity field in Figure 11 even for no air ejection case, which was probably because the cooling holes were not plugged up and some aerodynamic interaction happened between the holes and the flow. At plane E, where low speed region

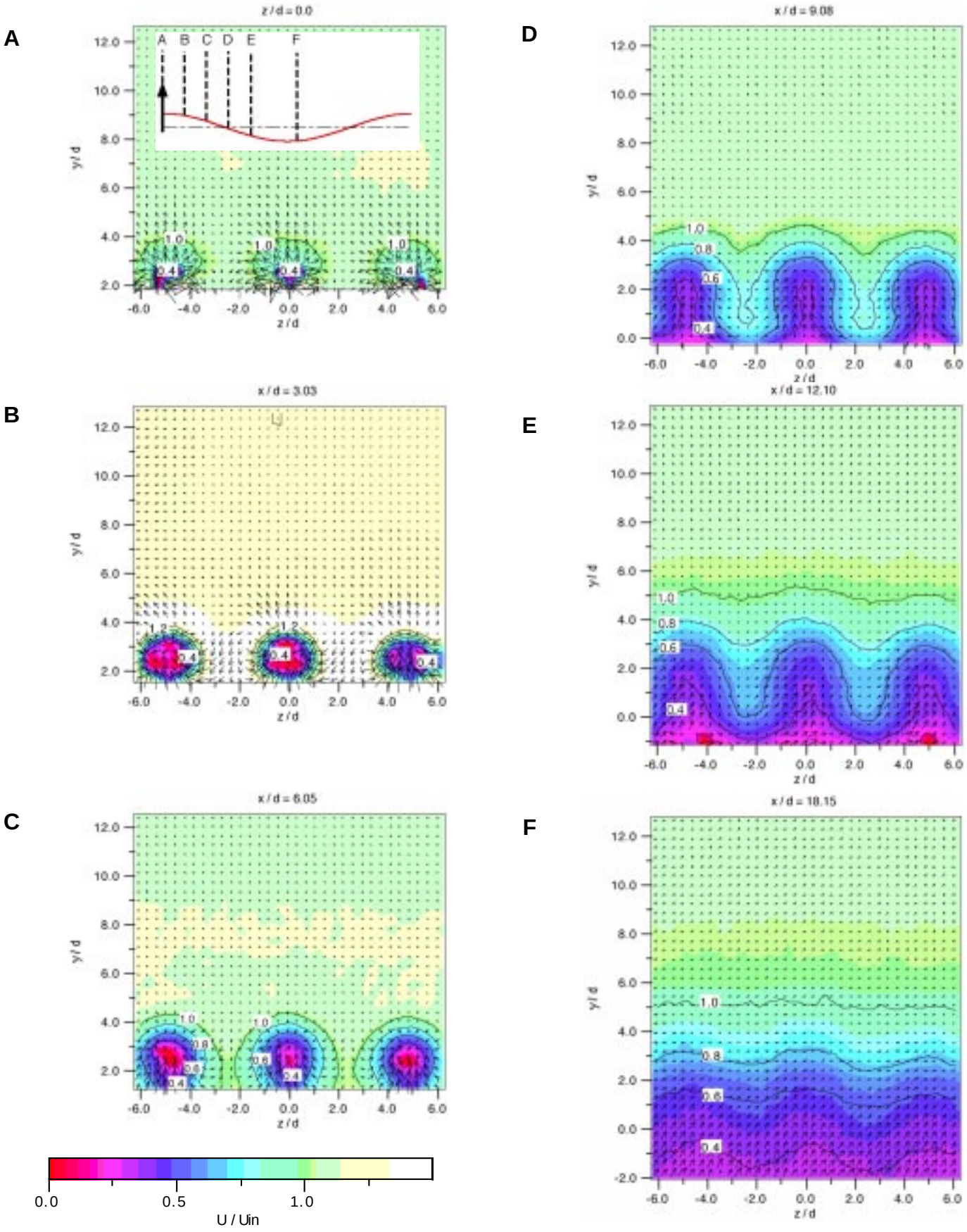

Figure 9 Contours of velocity magnitude on the measurement planes normal to the main flow direction, in conjunction with the secondary velocity vectors in the case of air ejection from the upstream cooling holes (m = 2.0)

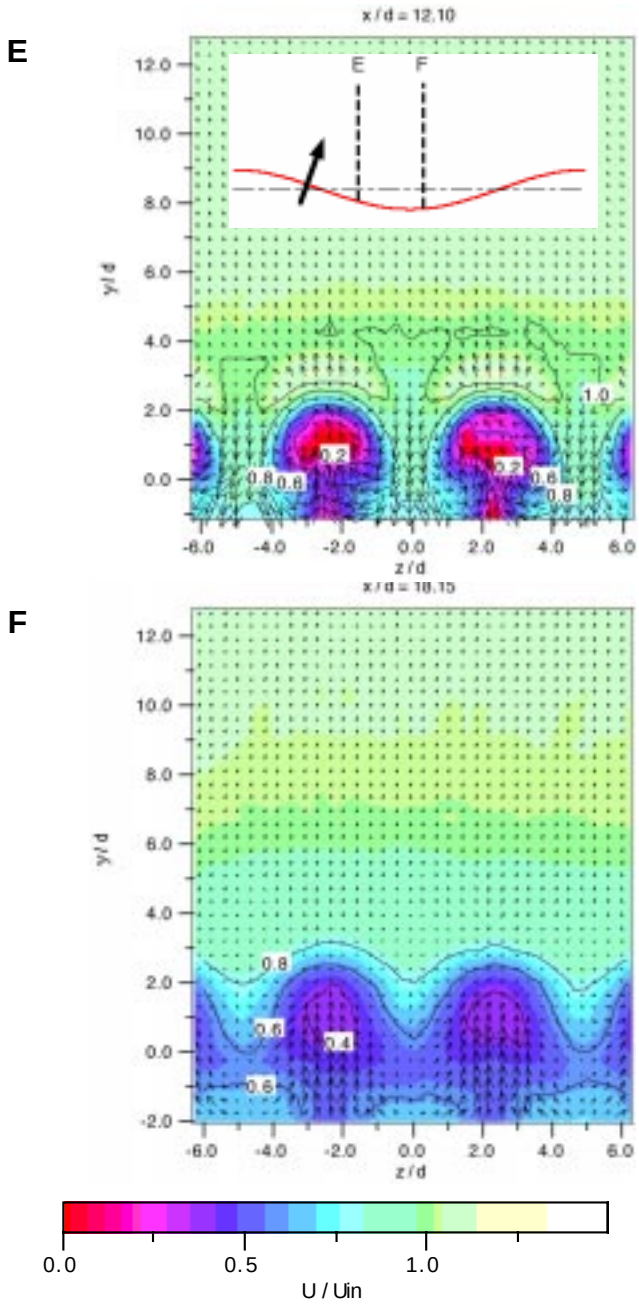

Figure 10 Contours of velocity magnitude on the measurement planes normal to the main flow direction, in conjunction with the secondary velocity vectors in the case of air ejection from the downstream cooling holes (m = 2.0)

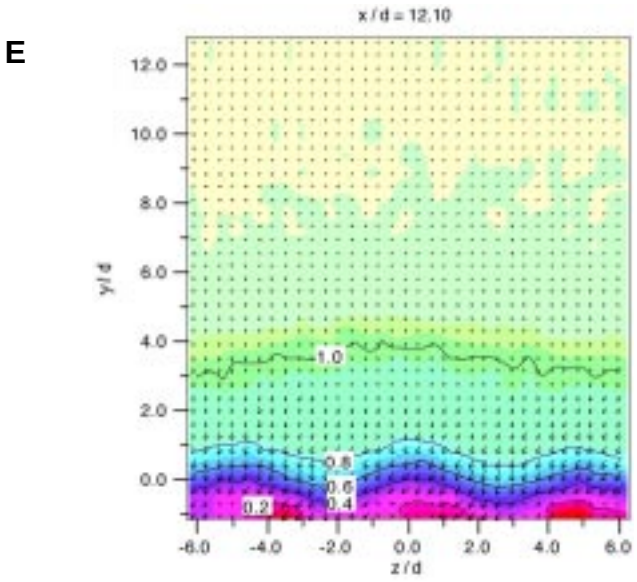

Figure 11 Contours of velocity magnitude on the measurement planes normal to the main flow direction, in conjunction with the secondary velocity vectors in the case of no air ejection

became visible under y/d = 0.0 in the case of no air ejection, the low momentum air near the wall was sucked up and seemingly merged with the wake of the jet and high momentum air from the main flow was drawn in towards the wall due to the vortical motion of the jet. This led to the appearance of mushroom-shape low speed region. At plane F, further downstream from the cooling hole concerned, the vortical structure observed at plane E considerably weakened and only upward motion still remained behind the jets.

The results from the test cases using single row ejection indicate a possibility that the upward motion behind the jet was generated not only by the vortical structure around the jet but by any other mechanisms such as pressure gradient from the near-wall to the upper edge of the jet, or entrainment effect.

Two Rows Ejection Figure 12 shows the results for the two rows ejection case with m = 2.0. Velocity fields ahead of the downstream row of the cooling holes (from plane A to plane C) were almost the same with those obtained in the upstream ejection case as shown in Figure 9. It is evident in Figure 12 that the jets from the downstream cooling holes significantly interacted with the upstream jets. The downstream jets were ejected between the two neighboring upstream jets, accompanying downwash outside the jets which was against the upward motion associated with the upstream jets as can be seen on plane D in Figure 12. As a result, the upward motion behind the upstream jets were almost eliminated. Furthermore, vortical structure around the downstream jets, which had been observed in the case of the single row ejection (plane E in Figure 10), disappeared on plane E in Figure 12, and only upward flow with slight skewness from the vertical direction remained behind the downstream jets. The interaction between the upstream and downstream jets promoted the flow field to be uniform up to the location of plane F.

Figure 13 presents some of the results of the velocity measurements for m = 4.0. As a whole, the flow field disturbed by the jets from the two rows of the cooling holes resembled that of m = 2.0. However, as can be easily imagined, the jets with this higher blowing ratio penetrated the main flow deeper than those of m = 2.0, so that the top of the jet reached about y/d = 8, while the jet of m = 2.0 reached about y/d = 6. Furthermore, these jets generated more intense vortical structure around them, promoting upward motion inside the jet wakes as well as downwash outside the wakes. This was, without doubt, detrimental to the corrugated liner cooling and is discussed in more detailed in the following section.

Temperature Measurements

Measurements on y-z planes Figure 14 shows non-dimensional temperature distributions obtained on the y-z planes in the case of two rows ejection for m = 2.0, in conjunction with the corresponding velocity vectors. It appears that high temperature zones in this figure

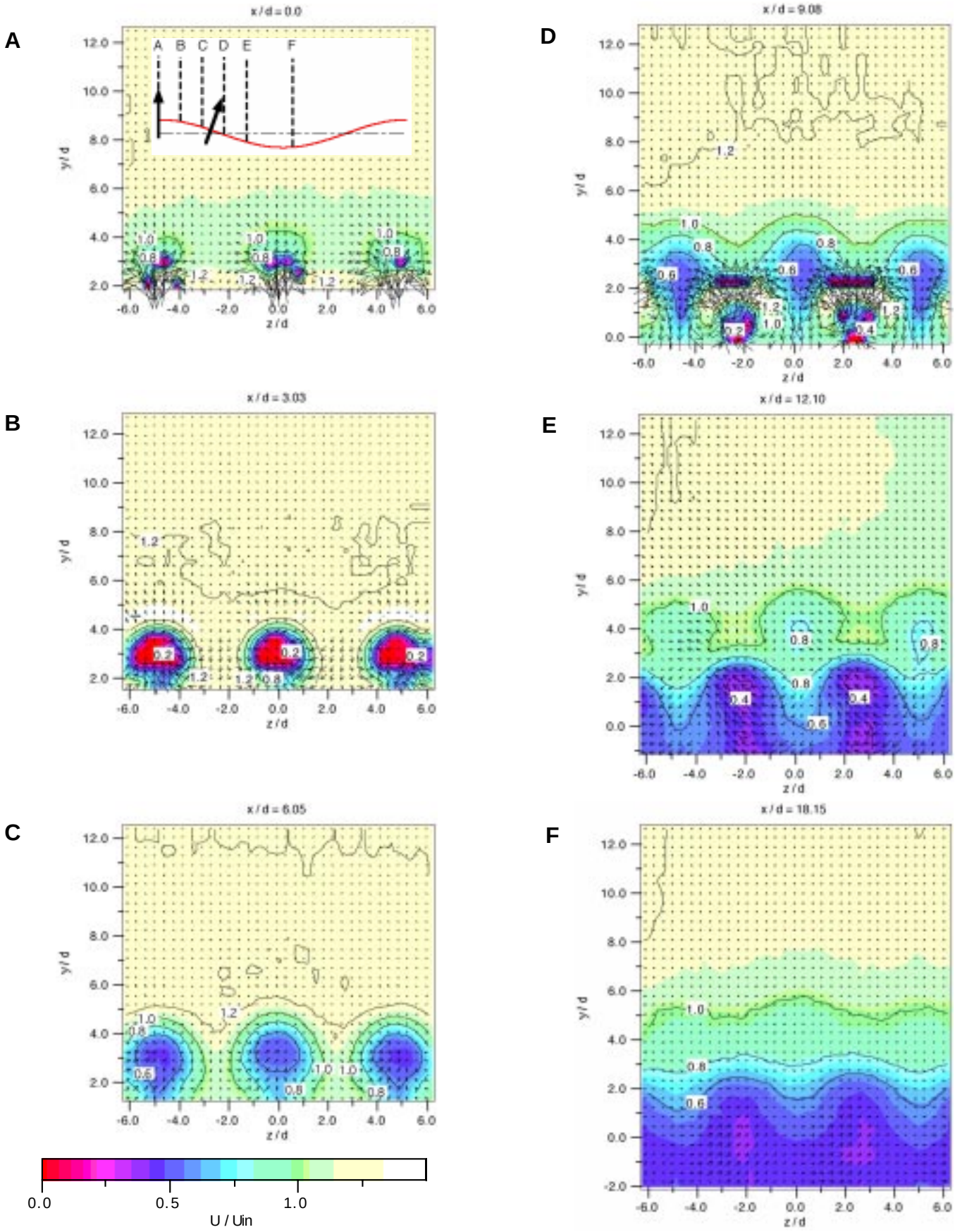

Figure 12 Contours of velocity magnitude on the measurement planes normal to the main flow direction, in conjunction with the secondary velocity vectors in the case of air-injection from two rows of the cooling holes (m = 2.0)

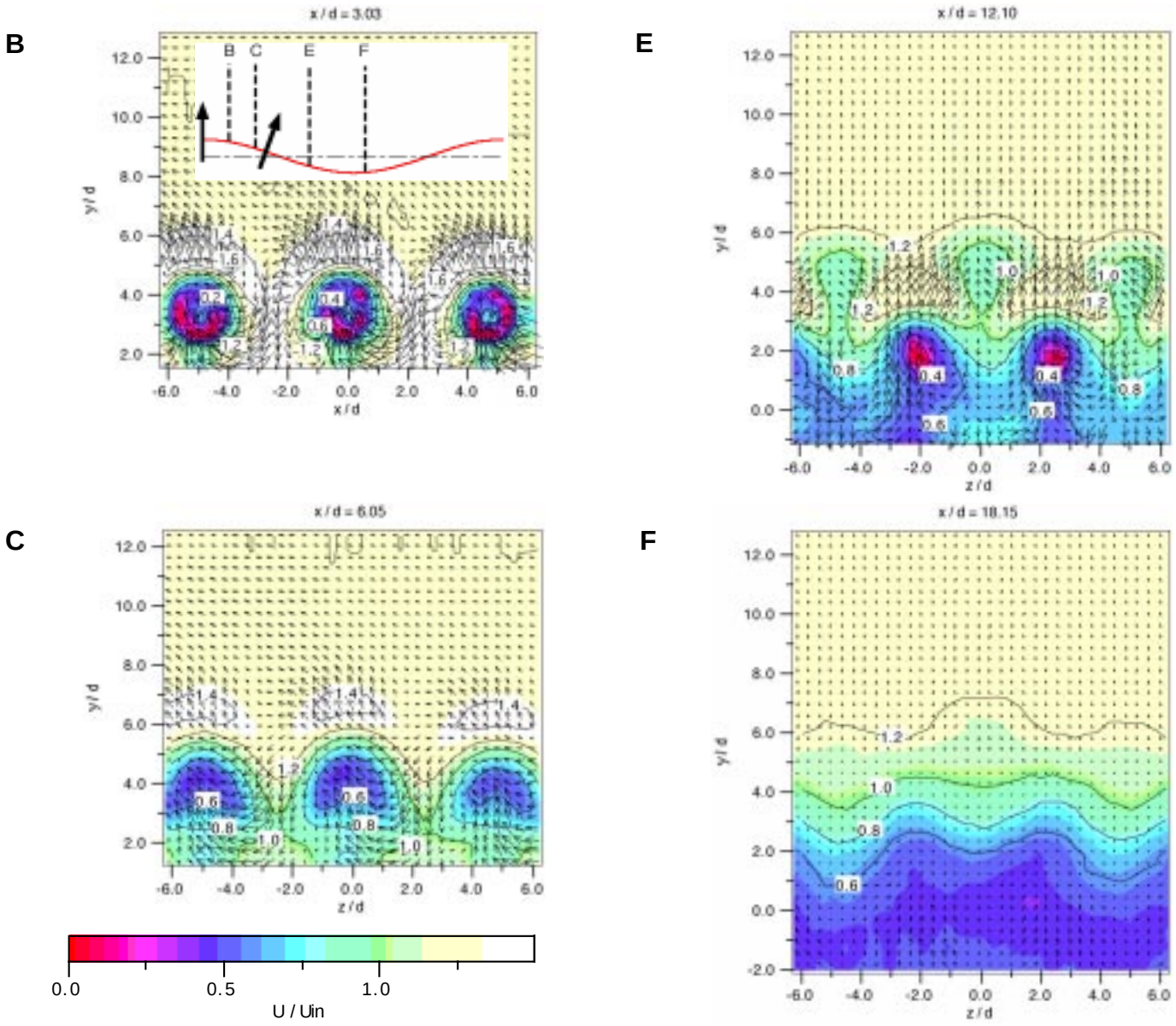

Figure 13 Contours of velocity magnitude on the measurement planes normal to the main flow direction, in conjunction with the secondary velocity vectors in the case of air-injection from two rows of the cooling holes (m = 4.0)

almost correspond to the air ejected from the upstream row of cooling holes. The jets took the shape of a semi-circle on plane A. On plane B, the jets slightly raised themselves from the wall mainly due to the effect of the upward velocity vectors induced by the counter-rotating vortices, showing rapid diffusion of the temperature. Thereafter, because of the effect of the descending surface, the high temperature zones extended vertically to the wall on plane C, while the location of the top of the jet remained unchanged. After the ejection from the downstream cooling holes (on plane D), the jets clearly exhibited clear kidney-like shape as reported by other investigations. However, these distinct structures quickly disappeared on plane E. It is rather surprising in plane F that only within about 18 times hole diameter distance from the upstream row the temperature field became almost uniform in the spanwise direction and got vertically stratified, which is definitely favorable to the wall cooling.

Figure 15 demonstrates the effect of higher blowing ratio onto the temperature field (m = 4.0). Due to the larger jet momentum, the high temperature zones of kidney-like shape were completely lifted off from the wall and eventually the fluid with relatively low temperature slipped under the jets, as seen on plane B. Further downstream (plane C), the jets slightly spread with some diffusion, however, since the cores of the jets remained at the same positions, the ejected air hardly reached the wall surface. Distinct kidney-shaped high temperature zones coming from the downstream row of the cooling holes appeared on plane D, accompanying intense upward motion. These zones had merged on plane E and became considerably uniform in the spanwise direction on plane F. In contrast to the case of m = 2.0, the temperature distribution for m = 4.0 had the layer of maximum value at the location apart from the wall, which was not desirable from the standpoint of the wall cooling.

Film Effectiveness on the Corrugated Wall As previously explained, film effectiveness on the corrugated surface could be determined by extrapolating the near-wall temperature data to the wall. Figure 16 shows contours of the film effectiveness obtained for m = 2.0 over

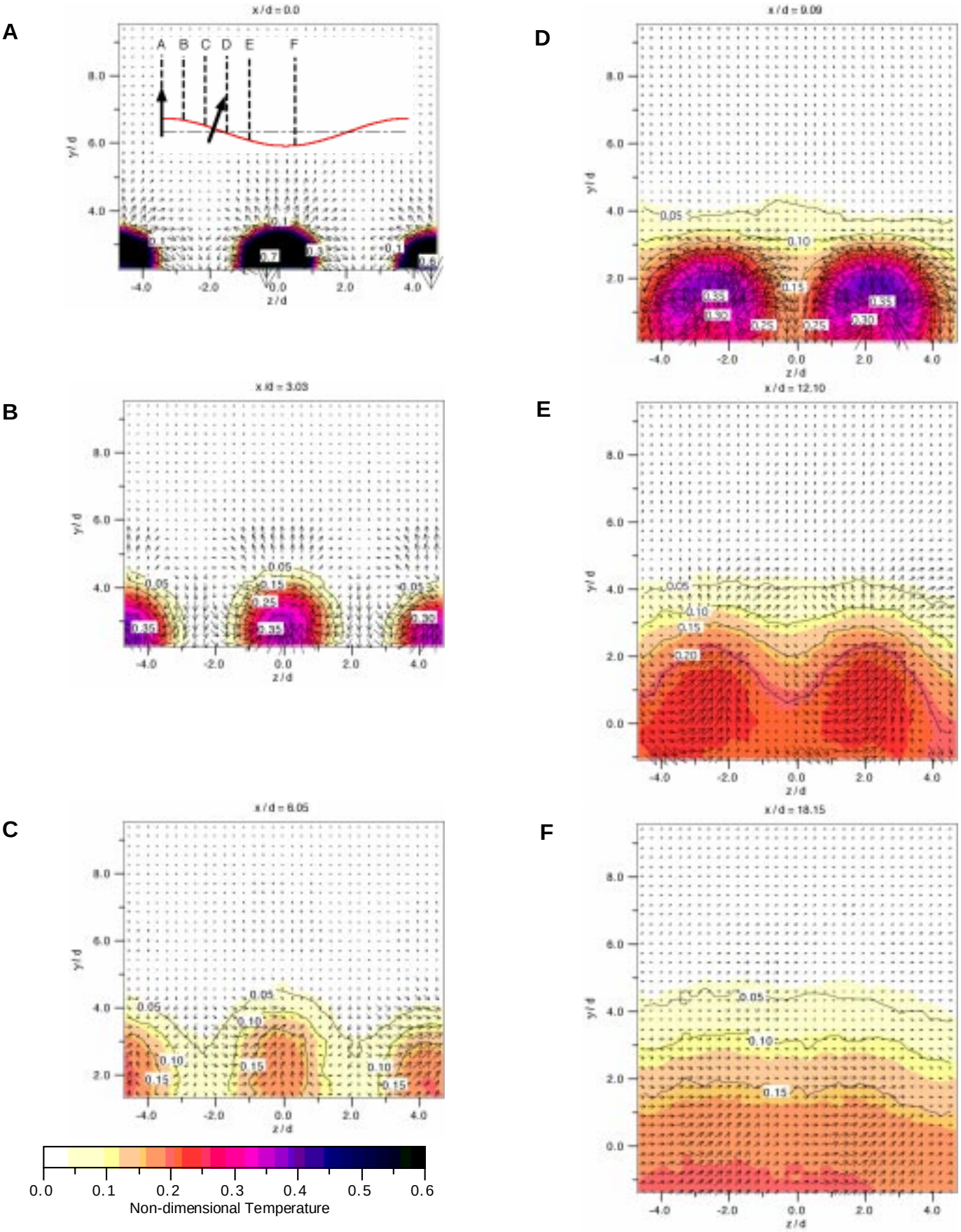

Figure 14 Contours of non-dimensional temperature on the measurement planes normal to the main flow direction, in conjunction with the secondary velocity vectors in the case of air-injection from two rows of the cooling holes (m = 2.0)

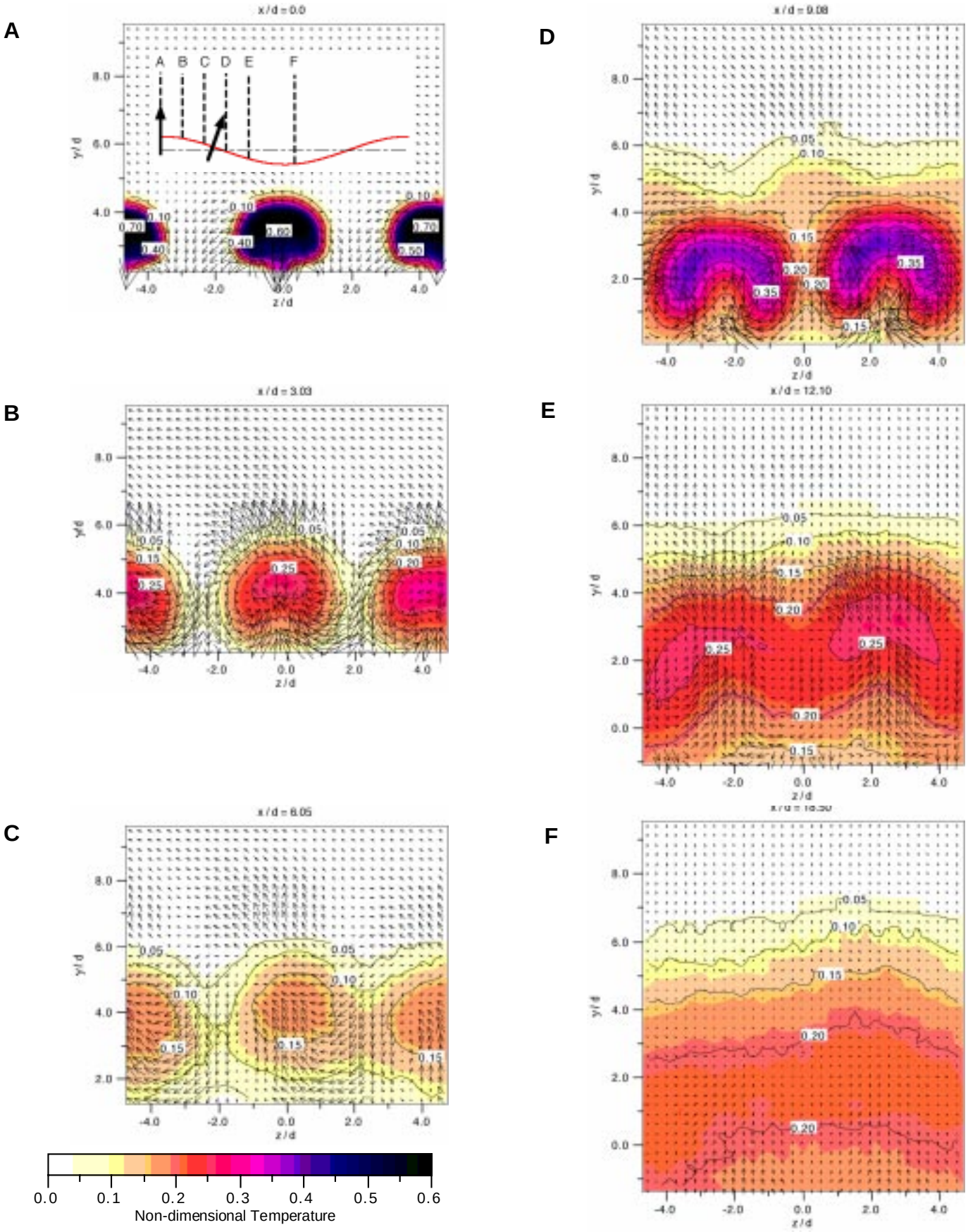

Figure 15 Contours of non-dimensional temperature on the measurement planes normal to the main flow direction, in conjunction with the secondary velocity vectors in the case of air-injection from two rows of the cooling holes (m = 4.0)

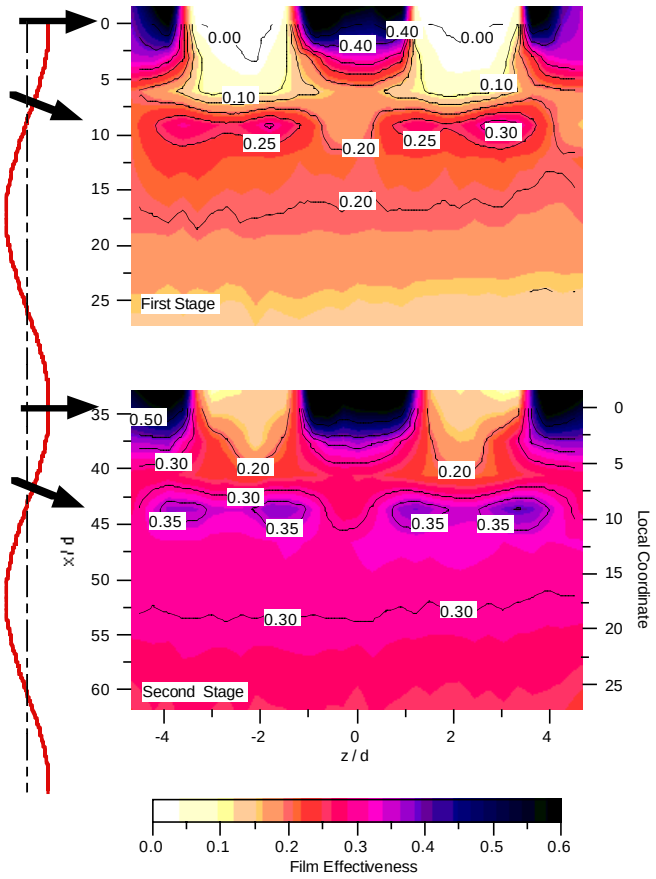

Figure 16 Contours of film effectiveness over the two-wavelength corrugated surface (m=2.0)

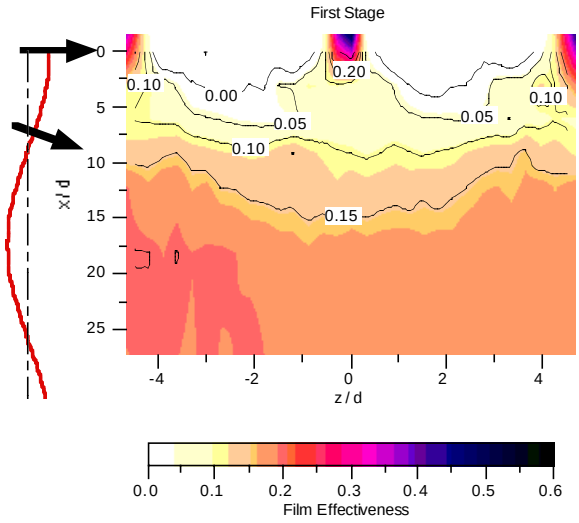

Figure 17 Contours of film effectiveness over the one-wavelength corrugated surface (m=4.0)

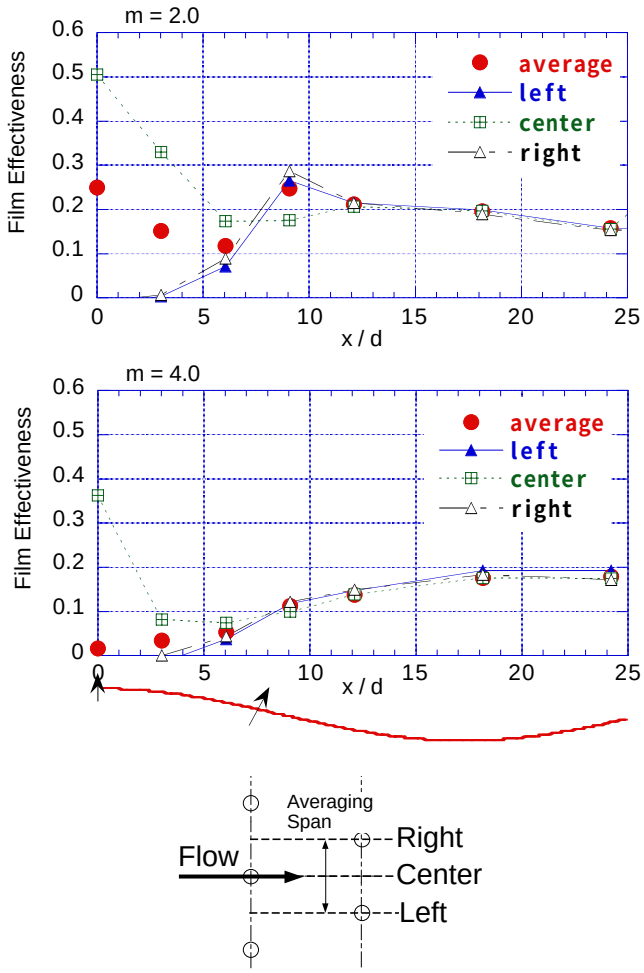

Figure 18 Averaged and local film effectiveness distributions (upper : m = 2.0 / lower : m = 4.0)

the two-wavelength range of the wall, which was projected onto the x-z plane. On the first wave of the corrugated wall, the highest film effectiveness was achieved around the upstream cooling holes, while virtually no-cooled regions emerged between the two neighboring holes. Just after the downstream cooling holes ($x/d \cong 10$), there appeared two peaks because the high temperature air took the kidney-like shape near the wall. Thereafter, the film effectiveness quickly became uniform. It appears that the corrugated surface helped a quick mixing of the ejected air with the surrounding air through the mechanism of the interaction between the jets and the low momentum fluid lying over the valley of the corrugated wall. Contours of the film effectiveness on the second wave of the corrugated wall looked like those on the first wave, except for the effect of the incoming flow with elevated temperature ($\eta \cong 0.15$). It is easily imagined that this effect accumulated wave by wave so that one could attain higher film effectiveness further downstream, as will be shown later. Figure 17 is also the film effectiveness contours for m = 4.0. In contrast to the case for m = 2.0, any footprints of this higher air ejection were hardly recognizable from this figure due to the lift-off effect of the high- momentum jets. As a whole, the film effectiveness gradually increased with the streamwise distance, and it reached the maximum near the end of the wave of the corrugated surface.

Figure 18 displays local film effectiveness distributions collected on the lines passing across the upstream cooling hole or the downstream cooling holes in the first wave for m = 2.0 (upper) and m =

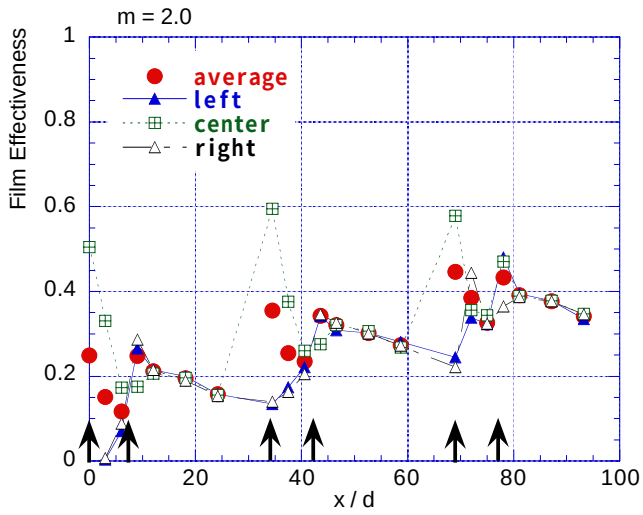

Figure 19 Averaged and local film effectiveness distributions over 3 wavelengthes of the corrugated surface (m = 2.0)

4.0 (lower) , which were designated 'Center', 'Left' or 'Right', as shown in the explanatory schematic of Figure 18. Averaged film effectiveness over the one pitch of the cooling holes are also shown in this figure. For m = 2.0 there appeared significant non-uniformity in the film effectiveness after the upstream cooling holes. Such non-uniformity completely vanished at x/d = 12 so that the local values agreed with the averaged value, then the film effectiveness gradually decreasing towards the downstream. The averaged film effectiveness reached a minimum just before the downstream cooling holes, followed by a maximum ($\eta \cong 0.26$). For m = 4.0, except for just behind the upstream cooling hole, only very low film effectiveness was attained over the zone where the secondary air was ejected, i.e., the zone ranging from x/d = 0 to x/d = 10. Accordingly, the averaged film effectiveness was at a very low level there. The averaged value then exhibited a gradual increase approaching to about 0.2, which was slightly higher than that attained for m = 2.0 at the most downstream location.

Figure 19 shows local and averaged film effectivenesses over three wavelengths of the corrugated surface. The film effectivenesses gradually increased with the streamwise distance as seen in Figure 16, while profiles of them on every wave resembled each other. This accumulation effect of the upstream hot air caused considerably high film effectiveness, which was about 0.35 at the end of three waves of the corrugated surface.

To conclude, the corrugated wall, in particular, its valley sections enhanced lateral mixing, resulting in the spanwise uniformity of the film effectiveness just downstream of the cooling holes. In this sense application of corrugated walls is not restricted only to aeroengine augmentors. However, since geometrical parameters adopted in the present experiments were limited and the free-stream turbulence was lower than that encountered in actual engines, further studies are needed to understand these effects upon the aerodynamics of the air ejection as well as the film effectiveness over the corrugated wall, then seeking another possibility of corrugated walls with air ejection as a cooling device.

CONCLUSIONS

This paper described the aero-thermo characteristics of the secondary air ejected into the primary flow from two rows of discrete cooling holes on the corrugated test model. The experimental findings through the present work can be summarized as follows:

(1) It was found from the velocity vectors on the y-z measurement planes that the vortical structure associated with the air ejection quickly attenuated while the upward movement induced inside the jet wake regions remained as it was until far downstream of the jet.

(2) Low momentum fluid region observed over the valley of the corrugated surface almost disappeared due to the mixing with the primary flow which was promoted by the interaction between the jets and the flow over the valley. These complicated interaction eventually weakened the coherent structure associated with the ejected air so that the flow field became almost uniform by the end of the first wave of the corrugated wall.

(3) The temperature measurements revealed that for the blowing ratio m = 2.0, which was near the design point, high temperature regions associated with the jets exhibited slight lift-off from the wall, taking the kidney-like shape. After the downstream cooling holes, the temperature field quickly became stratified in the vertical direction with horizontal uniformity. In the case of m = 4.0, the ejected air penetrated the primary flow due to its higher momentum, showing the noticeable lift-off from the wall. This lift-off brought about the appearance of low temperature zone near the wall.

(4) The air ejection for m = 2.0 attained a relatively high film effectiveness over the corrugated surface except near the upstream cooling holes. The accumulation of the incoming hot air from the upstream wave realized much higher film effectiveness on the far-downstream corrugated surface. In contrast, the ejected air m = 4.0 exhibited poor performance in film effectiveness due to its lift-off effect.

ACKNOWLEDGMENTS

The authors would like to express their gratitude to S. Yamawaki for his useful discussion to the present study. T. Nakano should be also acknowledged for his invaluable efforts contributed to this study.

References

1. Henn, D. S. and Sykes, R. S., 1999, "Large-Eddy Simulation of Flow over Wavy Surfaces," Journal of Fluid Mechanics, Vol. 383, pp. 75-112.
2. Lee, B. S., Kang, I. S. and Lim, H. C., 1999, "Chaotic Mixing and Mass Transfer Enhancement by Pulsatile Laminar Flow in an Axisymmetric Wavy Channel," International Journal of Heat and Mass Transfer, Vol. 42, pp. 2751-2581.
3. Russ, G. and Beer, H., 1996, "Heat Transfer and Flow Field in a Pipe with Sinusoidal Wavy Surface - I: Heat and Mass Transfer," International Journal of Heat and Mass Transfer, Vol. 40, pp. 1061-1070.
4. Sugiyama, H., Akiyama, M. and Yanagisawa, K., 1997, "Numerical Simulation of Turbulent Flow in a Channel with Large-Amplitude Wavy Surfaces," JSME Transaction, Vol. 63, pp. 2659-2665.
5. Ohta, T., Miyake, Y. and Kajishima, T., 1998, "Direct Numerical Simulation of Turbulent Flow in a Wavy Channel: 1st Report, Characteristics of Flow Field," JSME Transaction, Vol. 64, pp. 2094-2101.
6. Shinbo, K., Koide, Y., Kashiwagi, T., Funazaki, K. and Igarashi, T., 1997, "Research of Heat Transfer of a Liner for Afterburner," 33rd AIAA/ASME/SAE/ASEE Joint Propulsion Conference and Exhibition, AIAA 97-3005.
7. Kline, S. J. and McClintock, F. A., 1953, "Describing Uncertainties in Single Sample Experiments," Mechanical Engineering, Vol. 75, pp. 3 -
8. Leylek, J. H. and Zerkle, R. D., 1994, "Discrete-Jet Film Cooling: A Comparison of Computational Results with Experiments," Trans. ASME Journal of Turbomachinery, Vol. 116, pp. 358 - 368.